



Published in final edited form as:

Opt Lett. 2013 September 1; 38(17): 3249–3252.

Pulsed-light imaging for fluorescence guided surgery under normal room lighting

Kristian Sexton^{1,*}, Scott C. Davis¹, David McClatchy III¹, Pablo A. Valdes^{1,2,3}, Stephen C. Kanick¹, Keith D. Paulsen^{1,2}, David W. Roberts^{2,3}, and Brian W. Pogue^{1,2,4}

¹Thayer School of Engineering at Dartmouth College, 14 Engineering Dr. Hanover, New Hampshire 03755, USA

²Geisel School of Medicine at Dartmouth College, 1 Rope Ferry Drive, Hanover, New Hampshire 03755, USA

³Section of Neurosurgery, Dartmouth-Hitchcock Medical Center, 1 Medical Center Drive, Lebanon, New Hampshire 03756, USA

⁴brian.w.pogue@dartmouth.edu

Abstract

Fluorescence guided surgery (FGS) is an emerging technology that has demonstrated improved surgical outcomes. However, dim lighting conditions required by current FGS systems are disruptive to standard surgical workflow. We present a novel FGS system capable of imaging fluorescence under normal room light by using pulsed excitation and gated acquisition. Images from tissue-simulating phantoms confirm visual detection down to 0.25 μM of protoporphyrin IX under 125 $\mu\text{W}/\text{cm}^2$ of ambient light, more than an order of magnitude lower than that measured with the Zeiss Pentero in the dark. Resection of orthotopic brain tumors in mice also suggests that the pulsed-light system provides superior sensitivity *in vivo*.

OCIS codes

(110.0110) Imaging systems; (110.2970) Image detection systems; (170.1610) Clinical applications; (170.3890) Medical optics instrumentation; (230.3670) Light-emitting diodes

Fluorescence guided surgery (FGS) has been used to expand the diagnostic information available to surgeons during tumor resection [1] by providing contrast based upon specific molecules. In a phase III trial, Stummer *et al.* reported a doubling of the complete resection rate in glioblastomas under FGS, leading to widespread neurosurgical adoption in Germany [1]. However, since the remitted fluorescence signal from tissue can be overwhelmed by room lighting, current state-of-the-art wide field commercial FGS systems generally require the operating room lights be turned off or severely dimmed during fluorescence mode imaging [2–5]. The lighting change in the surgical field interrupts clinical workflow and reduces the appeal of the technology to practicing surgeons. An FGS system capable of

imaging under normal room light conditions with high detection sensitivity would represent an important advance that could accelerate acceptance of the technology for molecular-guided intervention in surgical oncology.

In this Letter, we describe a novel FGS system developed specifically for imaging under room lights that exploits pulsed excitation light and time-gated detection. This approach has been used to suppress signals for *in vivo* multispectral fluorescence imaging. [6–8]. Pulsed-light imaging can also increase the speed of image acquisition in surgical applications where excitation power is likely to dictate the minimum acquisition time [6,7]. In the system presented here, the first realization is shown in the context of wide-field video-rate capable FGS imaging. The theoretical value of the instrument is highlighted and a direct comparison with an industry standard operating microscope is made using liquid tissue phantoms as well as *in vivo* studies.

The principle advantage of pulsed-light imaging is relatively simple; namely, that reducing acquisition time while maintaining the same radiant exposure reduces the contribution of background light in the signal. The effect in turn maximizes the dynamic range of the imaging system to the fluorescence signal and enables realtime background subtraction [9]. It can be illustrated by considering the detected signal, S_d , in the presence of both the excitation source and background light:

$$S_d = \int \varepsilon \cdot c \cdot \Phi \cdot E_{\text{ex}}(t) dt + \int f \cdot E_{\text{ex}}(t) dt + \int E_A(t) dt,$$

where E_{ex} is the irradiance from the excitation source, E_A is irradiance from ambient room light, t is integration time, c , ε , and Φ are the concentration, molar extinction coefficient and quantum yield of the fluorophore, respectively, and f is some factor for nonspecific signal resulting from excitation light. Figure 1A illustrates this principle by plotting S_d as a function of time for two systems, one which provides a fixed excitation irradiance and the other, a theoretical construct, which provides a fixed radiant exposure, H , where $H = \int E_{\text{ex}}(t) dt$, both in the presence of a constant background intensity. The detected signal includes the sum of contributions from excitation and background light that must remain below some maximum value for the system to avoid saturation (here chosen to be 16 bits). At the same time, the portion of the detected signal from the fluorophore must be sufficiently above the nonspecific background signal produced by excitation light to provide acceptable contrast-to-noise ratio. The fact that the nonspecific excitation background signal (generally a combination of excitation light leakage and nonspecific fluorescence) is a function of excitation power prevents an increase in excitation power from producing a directly proportional increase in contrast to noise. However, at the lowest fluorescent levels, the increased signal that results from a greater E_{ex} may mean the difference between detection and loss of the desired signal within the noise floor. The tradeoffs are evident in Fig 1B, where both the background subtracted signals and the sum of nonspecific excitation background and noise for the two systems are plotted. The presence of strong background lighting prohibits the common solution of simply using longer imaging times to achieve adequate fluorescence signal. From a theoretical standpoint, the graph makes it clear that the optimum system provides just enough irradiance to remain just below saturation at the

shortest possible acquisition times, which both maximizes fluorescence to nonspecific excitation background signal as well as minimizes imaging time. However, practical limits dictate the minimum exposure time of the camera as well as the maximum irradiance that the light source can provide.

Critical to maintaining radiant exposure, as integration time decreases the ability to produce light at adequate intensity while also maintaining exposure within the maximum permissible (MPE) limits, the American National Standard (ANSI) Z136.1–2000 specifies the MPE optical values for skin and eye. Given no published values specific to the surgical cavity, the skin limits could be used. The pulsed MPE values are the lowest of the single-pulse, multipulse, and average power limit as described in the ANSI standards, where average exposure cannot exceed the 200 mW/cm^2 limit for continuous illumination. At pulse widths below $1000 \mu\text{s}$, frequencies of $10\text{--}100 \text{ Hz}$ and imaging times on the order of hours, there is a distinct advantage to using pulsed light in regard to MPE. Pulsed light can deliver a considerably greater instantaneous power with the extent of the increase depending on the fraction of time that the tissue is exposed. For example, with an acquisition time of $500 \mu\text{s}$, a pulse frequency of 50 Hz , and an imaging time of 1 h , the MPE is dictated by the average power limit which allows each pulse to deliver up to 8000 mW/cm^2 . This enables the exposure for each pulse to be ~ 40 times the power allowed during continuous light imaging. As a result, the practical limit of pulsed wide-field illumination is the power of the light source. As long as the necessary power can be delivered, the same fluorescent signals can be obtained at increasingly shorter gate widths, which is essential for both suppressing background signal and achieving rapid acquisition rates.

The pulsed-light system described here is configured to image protoporphyrin IX (PpIX) under surgical conditions. It consists of a PI-MAX 3–1024 \times 256 camera ($26 \mu\text{m}$ pixel size) (Princeton Instruments, Acton, Massachusetts) attached to an articulating arm via a custom mounting plate. The camera utilizes a UV Generation II intensified CCD (ICCD), which is able to achieve exposure times on the order of microseconds rather than the milliseconds typical of a standard CCD or electron multiplying CCD (EMCCD) [4]. Light received from the tissue is collected by a 24 mm F1.8 lens (Sigma, Ronkonkoma, New York) and then passes through an eight-position high-speed filter wheel (Edmund, Barrington, New Jersey) before focusing on the sensor. The setup enables efficient light collection from the lens and uses standard $1.0 \text{ in. (2.54 cm)}$ diameter interference filters (here, a 700 nm filter with 40 nm FWHM from Omega, Brattleboro, Vermont) with the filter wheel providing the potential to image multiple fluorophores or perform multispectral imaging. Surrounding the lens is an excitation light positioning system capable of holding up to eight SpecBright pulsed LED area lights (ProPho-tonix, Salem, New Hampshire) to illuminate the surgical field. In this study, four 630 nm LED's filtered with $1.0 \text{ in. } 650 \text{ nm}$ short pass filters (Edmund Optics, Barrington, New Jersey) were used. The LEDs provide wide field illumination with a reasonably narrow bandwidth and relatively high power, and in pulsed mode can be overdriven to 10 times the maximum power achievable in continuous operation (provided the pulse is below 1 ms and the duty cycle is less than 5%). From 25 cm , this four-light system running in pulsed mode is capable of providing 360 mW/cm^2 at the tissue surface. In the experiments described here the ICCD was gated to allow a $500 \mu\text{s}$ exposures and was synchronized to the LED pulses with all systems controlled through Labview (National

Instruments, Austin TX). Dynamic background subtraction was performed in real time with each pulsed light acquisition being preceded by an equivalent acquisition in the absence of excitation light.

To compare system performance against a state of the art clinical FGS instrument, a direct sensitivity comparison with the Zeiss OPMI Pentero Blue 400 surgical microscope was conducted. Tissue-simulating liquid phantoms consisting of 1% intralipid, 1 mg/ml hemoglobin (Hemoglobin A0 ferrous stabilized human, Sigma-Aldrich) and serial dilutions of PpIX were examined with both systems. Imaging was completed in ambient lighting conditions ($\sim 125 \mu\text{W}/\text{cm}^2$) with the pulsed-light system but was performed in the dark following standard clinical practice using the Pentero operating microscope. The Pentero system excites PpIX with violet blue light ($\lambda = 405 \pm 5 \text{ nm}$), which coincides with the maximum absorption peak of the compound. Images from both systems as a function of PpIX concentration are presented in Figs. 2A-2C. Visible fluorescence images from the Pentero are shown as the surgeon would see them in Fig. 2A. Figure 2B shows only red channel intensities extracted from the Pentero RGB images, and Fig. 2C presents the pulsed imaging system images of the same phantoms. Contrast-to-noise ratios and raw signal detected for the two systems are shown in Figs. 2D and 2E, respectively, where red channel values from Fig. 2B were used to quantify the Pentero metrics.

Results demonstrate the superior sensitivity to PpIX of the pulsed imaging system, which is observed despite detection under ambient light versus a dark room for the Pentero. The minimum visible concentration of PpIX was $0.25 \mu\text{M}$ for the pulsed FGS system and $5 \mu\text{M}$ for the Pentero (the Pentero did detect concentrations as low as $1 \mu\text{M}$ when examining the red channel only). Detected signal and contrast to noise were linear with concentration for both systems with R^2 values of 0.99 or greater.

The performance of the two systems during tumor resection of gliomas was also compared. Orthotopic U251 tumors were implanted in athymic nude mice 19 days prior to surgical imaging. To confirm the presence of tumors, gadolinium-enhanced MR images were acquired one day prior to surgery. For surgical imaging, mice were injected with 100 mg/kg of 5-aminolevulinic acid (ALA) i.p. 2 h prior, which leads to accumulation of PpIX in tumor cells. Animals were anesthetized using isoflurane, placed in a stereotactic frame, and the skull cap removed to expose the brain. Mice were then imaged with the pulsed FGS system under room lights and the Pentero operating microscope in the dark.

The mouse in Figs. 3A-3D demonstrates video-rate imaging *in vivo* (Media 1) with the pulsed FGS system under room light conditions. The T_1 -weighted gadolinium-enhanced MR image exhibiting tumor around 400 mm^3 and below the surface is shown in Fig 3A. No fluorescence enhancement was observed prior to resection with the Pentero system (Fig. 3B); however, the deeper penetration of red light from the pulsed FGS system revealed subsurface tumor tissue (Fig. 3C). As resection proceeds and tissue above the tumor is removed, a clear increase in fluorescence is evident as the tumor is exposed (Fig. 3D), demonstrating the highly sensitive, video rate, and subsurface detection potential of the pulsed imaging approach.

Other mice in the study were sacrificed following initial *in vivo* imaging, brains were extracted and sliced into four coronal sections, which were then imaged with both systems, processed for histology into formalin fixed paraffin embedded sections, and hematoxylin and eosin (H&E) stained. A representative case is shown in Figs. 3E-3H. *Ex vivo* images in Figs. 3G and 3H show the presence of a fluorescent subsurface mass with both systems, which was confirmed as tumor with the corresponding H&E slide (Figs. 3E and 3F).

These results suggest that pulsed imaging and gated detection can be deployed to facilitate FGS under ambient lighting conditions and without the need for specialized room-light filtering. The system described herein was shown to be sensitive to lower concentrations of PpIX than the current state-of-the-art commercial fluorescence surgical microscope. Interpretation of sensitivity studies must take into account the difference in excitation wavelengths used by the two systems. The Pentero excites in the blue where PpIX excitation is far more efficient than in the red (30-fold higher molar extinction coefficient at 405 nm than at 63 nm). Additionally hemoglobin absorption at 405 nm is 600 fold greater than at 630 nm. Monte Carlo simulations showed that the remitted fluorescence intensity should two to three fold higher using 405 nm versus 630 nm excitation. Even with this disadvantage, the gated system had a far lower detection limit, which reinforces the value of pulsed imaging. Monte Carlo results also showed that 405 nm excitation produced substantially more surface-weighted measurements, with an average depth of fluorescence origin at 0.15 versus 1.02 mm for 630 nm excitation. These results further demonstrate the advantage of red light excitation for the detection of subsurface tumor sites.

Improved sensitivity during surgical resection of tumor is critical. Valdes *et al.* reported *in vivo* visual detection of PpIX with the Pentero down to $\sim 1.07 \mu\text{M}$, while *in vivo* quantitative human data indicated a requirement for a detection threshold of $0.18 \mu\text{M}$ (roughly six times lower) to provide positive predictive values in excess of 90% and a detection threshold of $\sim 0.02 \mu\text{M}$ (roughly 60 times lower) to achieve sensitivities in high-grade gliomas of $>90\%$. These studies demonstrated that advanced optical detection techniques for PpIX fluorescence that achieve improved sensitivity will positively impact the diagnostic accuracy of FGS, suggesting the need for more sensitive technologies (advanced quantitative techniques, 87% accuracy versus visible techniques, 66%, $p < 0.0001$) [10–12]. The pulsed FGS system demonstrated detection to the level of $0.25 \mu\text{M}$ in realistic phantoms. Additionally, the UV Gen II sensor used here has a quantum efficiency (QE) of only 6% at 700 nm while other available sensors have QEs up to 35% at 700 nm which should improve these results even further.

One limitation evident from the direct comparison with the Pentero is the poor resolution of the current pulsed-light system. This can easily be addressed with upgraded optics that take advantage of the full size of the ICCD. Further improvements could be achieved with the use of the imaging version of the same camera, the PI-MAX 3–1024i, in which the pixels are half the size. However, it must be noted that either of these changes could adversely affect contrast-to-noise ratios.

The use of the spectroscopy camera in these experiments not only resulted in lower resolution, but also in a lower frame rate, approximately seven frames per second (fps) in the

absence of binning. Readout time from the ICCD is the primary limiting factor in regard to achieving the highest possible frame rates. The imaging version of the PI-MAX III has considerably faster readout times. The imaging version can be mounted on this system and is capable of achieving frame rates of 56 fps with pixels binned to match the 26 μm pixel size of the spec-troscopy camera and up to 140 fps when a 256×256 ROI is used.

The fast acquisition of pulsed-light imaging also holds promise for spectrally resolved FGS techniques under development for quantitative imaging [11]. Current approaches, which require multiple images to construct a spectral image data cube, could be dramatically accelerated with this process. In recent years, significant advances in light filtered microscopes have occurred that allow NIR and narrowband optical imaging [3,4]. The principles developed here for pulsed imaging are syner-gistic with these other filtering methods and could be combined to maximize signal to background ratios.

The system and concepts described herein show considerable potential for enabling highly sensitive fluorescence imaging under normal room light conditions and also for detecting fluorescence at some depth *in vivo*. These advances may have considerable impact on improving efficacy in FGS as well as in moving the technology further into the clinic.

Acknowledgments

This work has been financially supported by NIH grants R01 CA109558 and P01 CA084203, and Department of Defense award W81XWH-09-1-0661.

References

1. Stummer W, Pichlmeier U, Meinel T, Wiestler OD, Zanella F, Reulen HJ. *Lancet Oncol.* 2006; 7:392. [PubMed: 16648043]
2. Handa T, Katare RG, Sasaguri S, Sato T. *Interact Cardiovasc Thorac Surg.* 2009; 9:150. [PubMed: 19423513]
3. Themelis G, Yoo JS, Soh KS, Schulz R, Ntziachristos V. *J Biomed Opt.* 2009; 14:064012. [PubMed: 20059250]
4. Troyan SL, Kianzad V, Gibbs-Strauss SL, Gioux S, Matsui A, Oketokoun R, Ngo L, Khamene A, Azar F, Frangioni JV. *Ann Surg Oncol.* 2009; 16:2943. [PubMed: 19582506]
5. Stummer W, Stepp H, Moller G, Ehrhardt A, Leonhard M, Reulen HJ. *Acta Neurochir.* 1998; 140:995. [PubMed: 9856241]
6. Andersson-Engels S, Klinteberg C, Svanberg K, Svanberg S. *Phys Med Biol.* 1997; 42:815. [PubMed: 9172261]
7. Andersson-Engels S, Johansson J, Svanberg S. *Appl Opt.* 1994; 33:8022. [PubMed: 20963019]
8. Svanberg K, Wang I, Colleen S, Idvall I, Ingvar C, Rydell R, Jocham D, Diddens H, Bown S, Gregory G, Montan S, Andersson-Engels S, Svanberg S. *Acta Radiol.* 1998; 39:2. [PubMed: 9498864]
9. Glaser AK, Zhang R, Davis SC, Gladstone DJ, Pogue BW. *Opt Lett.* 2012; 37:1193. [PubMed: 22466192]
10. Valdes PA, Leblond F, Kim A, Harris BT, Wilson BC, Fan X, Tosteson TD, Hartov A, Ji S, Erkmen K, Simmons NE, Paulsen KD, Roberts DW. *J Neurosurg.* 2011; 115:11. [PubMed: 21438658]
11. Valdes PA, Leblond F, Jacobs VL, Wilson BC, Paulsen KD, Roberts DW. *Sci Rep.* 2012; 2:798. [PubMed: 23152935]
12. Valdes PA, Kim A, Brantsch M, Niu C, Moses ZB, Tosteson TD, Wilson BC, Paulsen KD, Roberts DW, Harris BT. *J Neuro-Oncol.* 2011; 13:846.

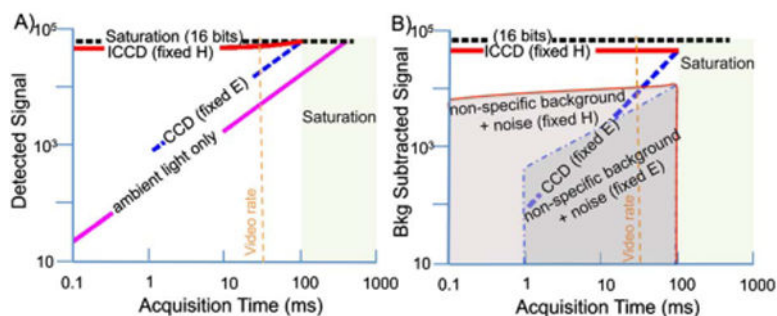


Fig. 1. Conceptual plots to illustrate the advantage of pulsed imaging and gated acquisition for low level fluorescence detection in the presence of high background lighting. A, Detected signal versus acquisition time for a standard CCD where excitation light remains constant (dashed blue), for an ICCD where excitation light increases proportionally as acquisition time decreases (red), and for ambient room light only with no excitation (pink). B, Background subtracted signal versus acquisition time for CCD (dashed blue) and ICCD (red) in the context of nonspecific background signal and noise for both fixed radiant exposure, H (red shading outlined in solid red) and fixed irradiance, E (blue shading outlined in dashed blue). Note that signal differences have been exaggerated to enable easy visualization.

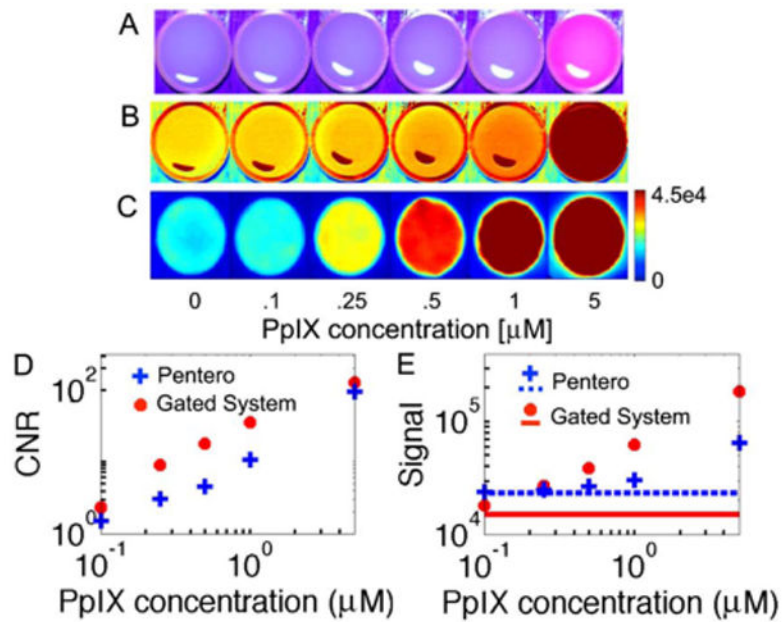


Fig. 2.

Fluorescence images of tissue-simulating phantoms containing different concentrations of PpIX. A, Zeiss Pentero surgical microscope (acquired in the dark) RGB images visible to the surgeon, B, Pentero images from the red RGB channel only, and C, background subtracted images from the pulsed imaging system in ambient lighting. (Note: pulsed images smoothed using a median filter and color scale on all images chosen to show maximum contrast and no images are saturated.) Phantom resolution, D, contrast to noise (calculated using central ROI in original images), and E, raw signal for both systems where solid and dashed lines indicate signal in absence of PpIX.

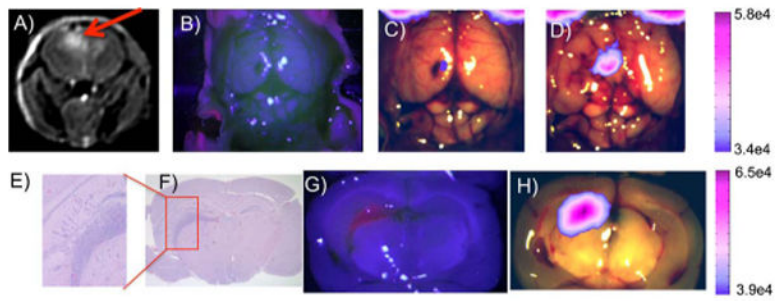


Fig. 3.

Images from two separate mice with orthotopic U251 glioma. A, Preoperative MRI T1-weighted with gadolinium contrast (red arrow indicates tumor location). B, *In vivo* image of exposed brain using the Pentero. C, Background subtracted fluorescent *in vivo* image of exposed brain from the current system prior to any resection and D, following resection and exposure of the tumor. Brain sections E and F, stained with H and E. G, Imaged with the Pentero and H, imaged with current pulsed-light system. (All pulsed-light fluorescent images overlaid on Pentero white light images use 60% thresholding and were obtained with room lights on.)